Proceedings of the XVII ECSMGE-2019
Geotechnical Engineering foundation of the future
ISBN 978-9935-9436-1-3

doi: 10.32075/17ECSMGE-2019-0310

XVII European Conference
ECSMGE 2019
Reykjavik
on Soil Mechanics
and Geotechnical Engineering

Numerical study on the efficiency of the insulation of borehole heat exchanger fields used for seasonal thermal storage

Etude numérique sur l'efficacité de l'isolation des champs d'échangeurs de chaleur des forages utilisés pour le stockage thermique saisonnier

H. Räuschel, O. Reul
Department of Geotechnical Engineering, University of Kassel, Germany

ABSTRACT: To prevent thermal energy losses of borehole heat exchanger (BHE) storages an insulation of the top surface of the storage is an option which brings the efficiency of such an insulation into focus. Numerical studies on insulated BHE storages show higher thermal gradients in the upper domain of the storage in comparison to storages without insulation. However, no significant gradient differences are noticeable at larger depths. Therefore, following numerical studies on the benefits of BHE storage insulations were carried out. A numerical heat load test was applied to investigate the advantage of different configurations of insulation and showed just slightly better performances of the insulated models.

RÉSUMÉ: Pour éviter les pertes d'énergie thermique des accumulateurs d'échangeurs de chaleur (BHE), une isolation de la surface supérieure de l'accumulateur est une option qui met en évidence l'efficacité d'une telle isolation. Des études numériques sur les entrepôts de BHE isolés montrent des gradients thermiques plus élevés dans le domaine supérieur de l'entrepôt par rapport aux entrepôts sans isolation. Cependant, aucune différence significative de gradient n'est perceptible à de plus grandes profondeurs. C'est pourquoi, après des études numériques sur les avantages des isolants de stockage BHE, des études numériques ont été réalisées. Un essai numérique de charge thermique a été appliqué pour étudier l'avantage de différentes configurations d'isolation et a montré des performances légèrement supérieures pour les modèles isolés.

Keywords: geothermal energy; borehole heat exchanger; insulation; seasonal thermal storage; efficiency

1 INTRODUCTION

Two third of the total heat energy consumption in Germany is used as domestic heat (Umweltbundesamt 2017). Hence, it is indispensable for the energy transition to develop new innovative residential quarters on the basis of a renewable heat energy supply. The combination of renewable energies with efficient supply technologies enables a significantly higher degree of sustainability for new housing areas.

The direct application of solarthermal energy by means of solar collectors is a cost-effective method of heat supply without direct emission of CO_2 or atmospheric particulate matter. One problem in the context of application of renewable energies via solar collectors for domestic heating and warm water is the heat energy supply during

the winter season. A high demand for thermal energy contrasts with a low energy supply. In Germany the seasonal availability of solar energy is limited to approximately 160 kWh/m² of global radiation in a summer month and to approximately 20 kWh/m² in a winter month (Deutscher Wetterdienst 2018). A possible solution to this problem could be the application of seasonal heat storage systems such as container heat storage, ground basin heat storage, borehole heat exchanger (BHE) storage or aquifer heat storage (Figure 1).

2 SEASONAL HEAT STORAGE BY MEANS OF BOREHOLE HEAT EXCHANGERS

A borehole heat exchanger (BHE) consists of vertical heat exchanger pipes and a footpiece installed in boreholes that usually reach depths up to 200 m (VDI 2001a).

Typically, single U-shape pipes (1U), double U-shape pipes (2U) or coaxial pipes composed of synthetics such as polyethylene (PE) are used as heat exchanger pipes. After placing the heat exchanger pipes inside the borehole, a thermally conductive and void-free backfilling has to ensure the contact between the pipes and the soil from the bottom to the top of the borehole. Inside of the heat exchanger pipes a heat carrier fluid (commonly an ethylene glycol-water mixture) circulates which extracts or transfers thermal energy from or to the underground, respectively.

The advantages of BHE storages compared to alternative storage systems (Figure 1) are the relatively low production costs and the possibility of the modular expandability (Al-Addous 2006). On the other hand, large storage volumes are required due to the low heat capacity of soil and rock compared to water. Moreover, BHE storages show relatively high heat losses, since the system can usually only be insulated on the ground surface.

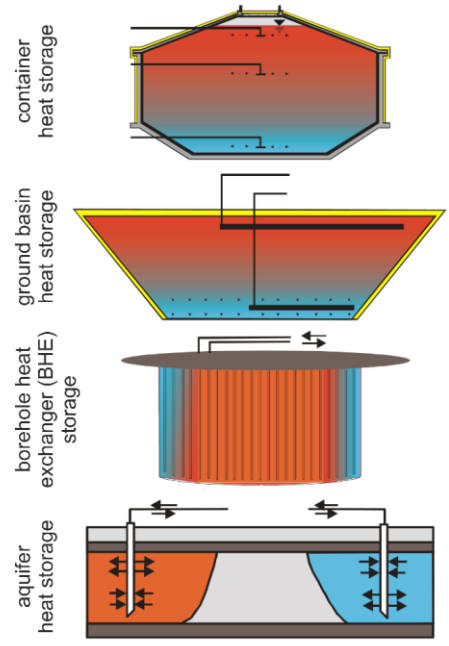

Figure 1. Systems for seasonal heat storage (after Ochs et al. 2007)

To reduce heat energy losses, it is recommended by VDI 4640 (VDI 2001b) to arrange the BHE circular in ground plan to minimize the surface-volume ratio of the storage. The BHE of a storage should be connected to each other in such a way that during summer the heat energy injection takes place from the inside to the outside and the heat energy extraction during winter in the opposite direction.

3 NUMERICAL STUDY

3.1 Setup of the numerical model

After Al-Addous (2006) one of the disadvantages of BHE storages are the relatively high heat energy losses in comparison to alternative systems. Because of the large volume and the in situ construction of BHE storages they can only be insulated on the top.

The aim of this study is to investigate the efficiency of an insulation on the top of BHE storages. For this task a numerical study by means of

a three-dimensional coupled finite element analysis was carried out to model heat energy injection and extraction of a BHE storage. The applied software FEFLOW (DHI 2015) is able to simulate the transport of matter and heat energy in porous media including conductive as well as convective heat energy transport.

The following model configuration was chosen as the basis for the study: number of BHE n_{BHE} = 96; distance between BHE s_{BHE} = 8 m; length of BHE L_{BHE} = 120 m; 2U-pipes connected in parallel mode on a rectangular BHE storage area of 42 m × 196 m; constant pump rate Q_{fluid} = 0.5 l/s.

The soil parameters applied in the numerical model are based on the geology of the city of Kassel, Germany. According to the geological map (HLUG 1969) the upper >100 m are dominated by the layers of the Upper Buntsandstein (as part of the Germanic Trias) consisting of shale and marlstone. Below the Middle Buntsandstein is located which in central Germany mainly consists of sandstone.

The main material properties of the two rock layers used in the finite element analyses are summarized in Table 1.

Table 1. Numerical model: Properties of the rock layers in the FE simulations

Property	Unit	Upper Buntsandstein	Middle Buntsandstein
$k_{f,h}$ / $k_{f,v}$	[m/d]	3.46×10^{-4}/ 3.46×10^{-5}*1	0.259/ 0.130*1
Φ	[-]	0.065*2	0.160*2
c_V	[MJ/m³/K]	2.25*3	2.20*3
λ	[J/m/s/K]	2.2*3	2.8*3
A_{tc}	[-]	0.760*4	0.872*5

$k_{f,h}$/$k_{f,v}$, hor./vert. permeability; Φ, porosity; c_V, vol. heat capacity; λ, thermal conductivity; A_{tc}, anisotropy of solid thermal conductivity

*1Domenico & Schwartz 1990; *2Matthess & Ubell 1983; *3VDI 2010; *4Midttømme et al. 1998; *5Hurtig 1965

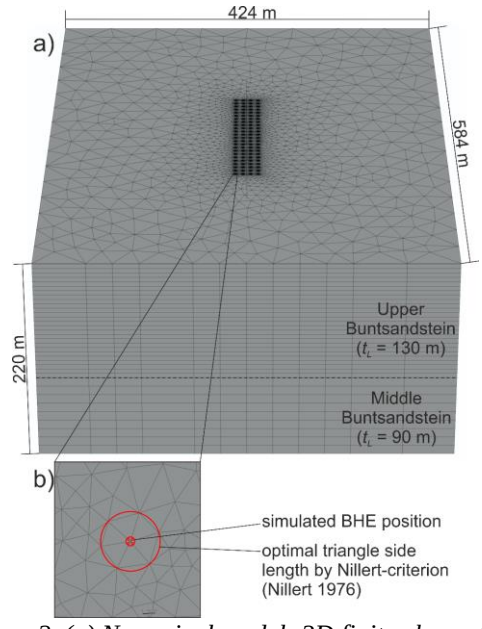

Figure 2. (a) Numerical model: 3D finite element model, (b) reduction of the BHE to an internal boundary condition (after Diersch et al. 2010)

Figure 2a shows the 3D finite element model comprising more than 600,000 elements and 300,000 nodes with the 96 BHE located in the model centre. The BHE are not discretized in detail but are reduced to an internal boundary condition (Diersch et al. 2010) applying the Nillert criterion (Nillert 1976) for the mesh discretization around a BHE (Figure 2b).

The model surface temperature $T_{surface}$ as well as the heat flux through the base of the model, q are held constant over time during the simulations with $T_{surface}$ = 10 °C (Meteonorm 2016) and q = 0.065 W/m² (LIAG 2016).

3.2 Numerical heat load test

3.2.1 General remarks

In a previous study (Reul et al. 2017) the influence of a 0.5 m thick foam glass layer insulation (see Table 3 for material properties) on the temperature distribution inside of a BHE storage has been investigated showing no significant influence except for the uppermost part of the storage.

Table 2. Heat load test setup of the numerical study

Phase	Duration [a]	Load
Heat energy injection	0.5	T_{in} = 60 °C
Heat energy extraction	1.0	P_{out} = 200 MJ/d/BHE

To investigate the efficiency of insulations of BHE storages a numerical heat load test was performed to compare different insulating materials and insulation thicknesses. The numerical heat load test consists of two phases (Table 2). Phase 1 covers a time span of t_{ph1} = 0.5 a during which every BHE is injected with a constant temperature of T_{in} = 60 °C. In Phase 2 with a duration of t_{ph2} = 1.0 a heat energy of P_{out} = 200 MJ/d is extracted from every BHE.

3.2.2 Variation of the insulating material

In a first step, different types of insulating materials have been compared to the default model without insulation. Materials which have been applied in BHE storage projects such as foam glass (Crailsheim, Germany, Nußbicker-Lux 2010), clay (Kungsbacka, Sweden, Hultmark 1982), lightweight expanded clay aggregate (Ispra, Italy, Nußbicker-Lux 2010), polystyrene XPS (Okotoks, Canada, Nußbicker-Lux 2010) and mussel shells (Braedstrup, Denmark, Bach 2012) have been investigated applying a constant layer thickness of 0.5 m. The thermal properties of the insulation materials are summarized in Table 3.

3.2.3 Variation of the insulation thickness

The second step involves a variation of the thickness t_{ins} of the insulating layer. Therefore, foam glass (Table 3) was chosen as initial material and stepwise increased in thickness (0.05 m – 0.10 m – 0.20 m – 0.30 m – 0.40 m – 0.50 m – 0.60 m – 0.80 m – 1.00 m) to be compared to the default model without any insulation.

Table 3. Thermal properties of tested insulation materials

Property	Unit	Foam Glass	Clay	Expanded clay	Polystyrene XPS	Mussel shells
c_V	[MJ/m³/K]	0.136 [*1]	1.55 [*2]	0.424 [*3]	0.051 [*1]	1.575 [*2]
λ	[J/m/s/K]	0.070 [*1]	0.500 [*2]	0.100 [*4]	0.035 [*1]	0.112 [*4]
A_{tc}	[-]	1 [*5]	0.8 [*5]	1 [*5]	1 [*5]	0.9 [*5]

c_V, vol. heat capacity; λ, thermal conductivity; A_{tc}, anisotropy of solid thermal conductivity
[*1]Ochs et al. 2004; [*2]VDI 2010; [*3]baupraxis-blog 2018; [*4]SAKRET 2018; [*5]estimated

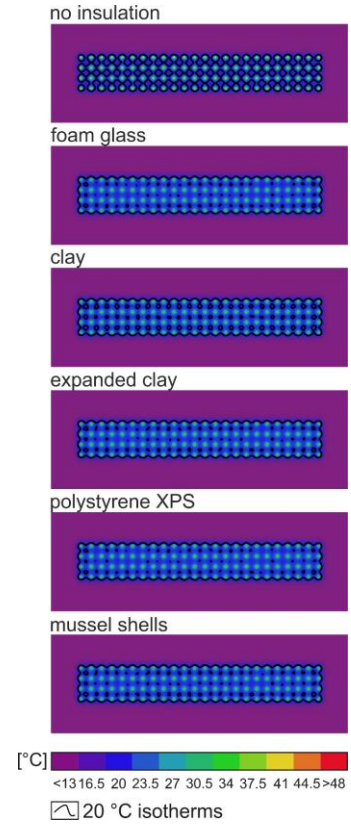

Figure 3. Temperature distribution in a depth of z = 5 m for different insulating materials after the heat energy injection (phase 1)

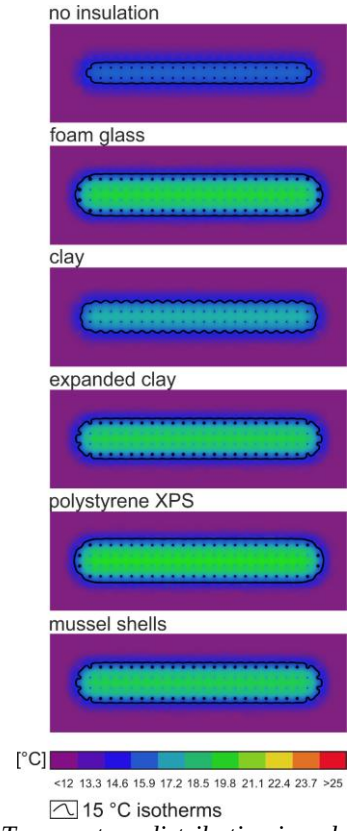

Figure 4. Temperature distribution in a depth of z = 5 m for different insulating materials after the heat energy extraction (phase 2)

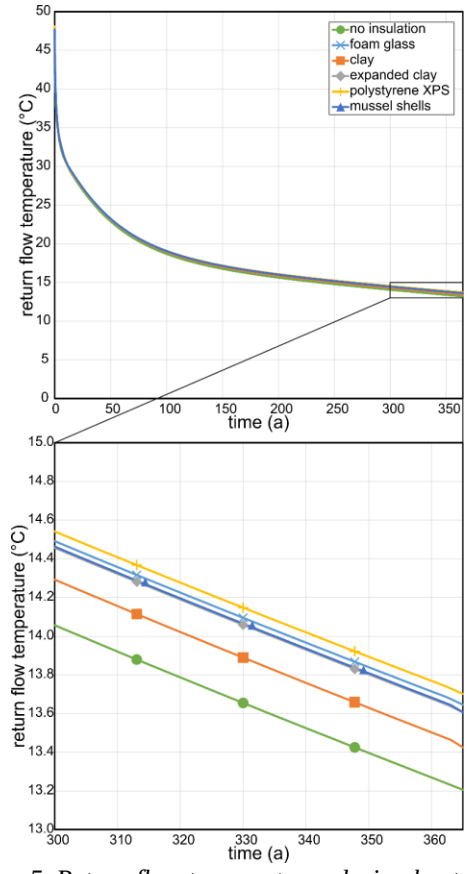

Figure 5. Return flow temperatures during heat energy extraction (phase 2) for different insulating materials

3.3 Results

3.3.1 Variation of the insulating material

Figure 3 and Figure 4 show the temperature distribution in a depth of z = 5 m for the tested insulating materials and for the default model without insulation. After the heat energy injection (phase 1; Figure 3) there are only negligible differences between the varying configurations. After the heat extraction (phase 2; Figure 4) the results become more heterogenous. As expected, the model without insulation shows the lowest temperatures followed by the clay-insulated model. The best insulation, i. e. the highest temperatures, can be identified for the models with foam glass and polystyrene models, respectively, at the top of the BHE.

Figure 5 shows the development of the return flow temperatures of the heat carrier fluid during heat energy extraction (phase 2) confirming the results of Figure 4.

The return flow temperatures are mainly controlled by the thermal conductivity of the insulation material (Table 3). Decreasing thermal conductivity obviously yields rising return flow temperatures with the maximum values for polystyrene XPS. However, the temperature difference between the polystyrene XPS and the uninsulated model amounts to only $\Delta T \approx 0.5$ K.

3.3.2 Variation of the insulation thickness

Figure 6 and Figure 7 show the temperature distribution in a depth of z = 5 m below the top of

the BHE for varying thickness t_{ins} of a foam glass insulation. After the heat energy injection (phase 1; Figure 6) the temperature distribution is almost identical for the various configurations. Similar to the variation of insulation materials the results show a larger deviation after the heat energy extraction (phase 2; Figure 7). As expected the temperatures increase with increasing insulation thickness, which is confirmed by the development of the return flow temperatures of the heat carrier fluid during heat energy extraction plotted in Figure 8.

The temperature difference between the foam glass with t_{ins} = 1.00 m and the uninsulated model amounts to $\Delta T \approx 0.5$ K (Figure 8). However, it is interesting to note that placing a foam glass layer with t_{ins} = 0.05 m yields a temperature increase of $\Delta T \approx 0.16$ K while increasing the thickness from t_{ins} = 0.50 m to t_{ins} = 1.00 m cause only an increase of $\Delta T \approx 0.06$ K.

For the investigated BHE storage and t_{ins} = 1.00 m a volume of $V_{ins} \approx 8{,}000$ m³ of insulation material would be required. Assuming costs of approximately 75 €/m³ for foam glass (GEOCELL 2018) this would yield material costs of approximately 600,000 € for the top insulation of the BHE storage. Additionally, costs for example for geosynthetic layers at the base and on top of the foam glass insulation or for a drainage system may apply.

4 CONCLUSIONS

The numerical heat load tests show a temperature difference of the return flow temperatures of the heat carrier fluid between the uninsulated model and the best insulating material polystyrene XPS of $\Delta T \approx 0.5$ K. The same temperature difference can be observed between the uninsulated model and the model insulated with a 1 m thick foam glass layer on top of the BHE storage.

The increased temperature in the BHE storage and the resulting increased return flow temperatures of the heat carrier fluid will increase the efficiency of the heat pump fed by the BHE field. However, the higher efficiency of the heat pump and the resulting lower operating costs of the system over the service life of the system must be compared with the costs for the insulation which are not negligible.

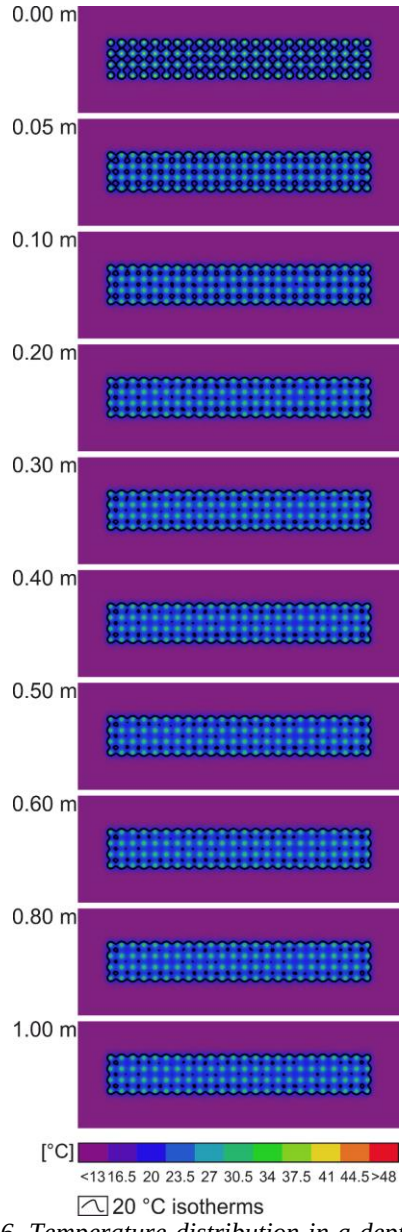

Figure 6. Temperature distribution in a depth of z = 5 m after the heat energy injection (phase 1) for varying thickness of a foam glass layer

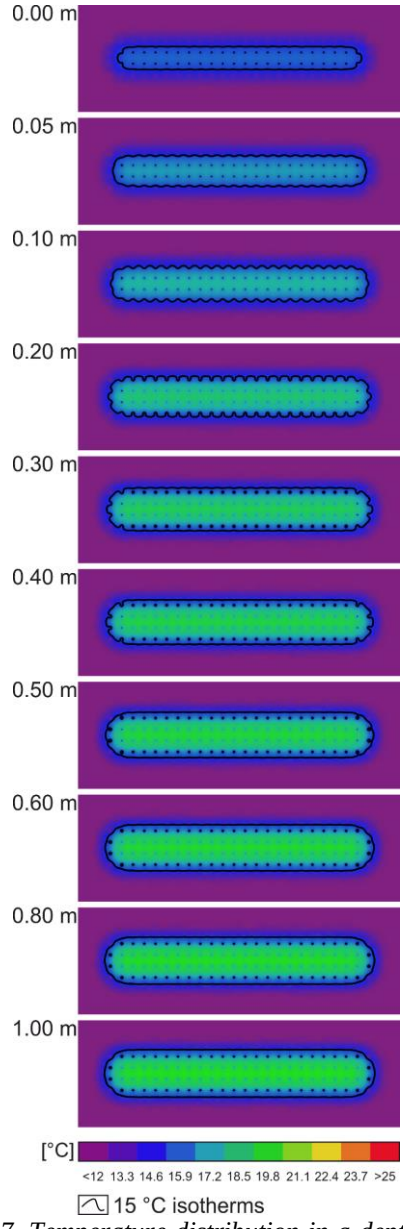

Figure 7. Temperature distribution in a depth of z = 5 m after the heat energy extraction (phase 2) for varying thickness of a foam glass layer

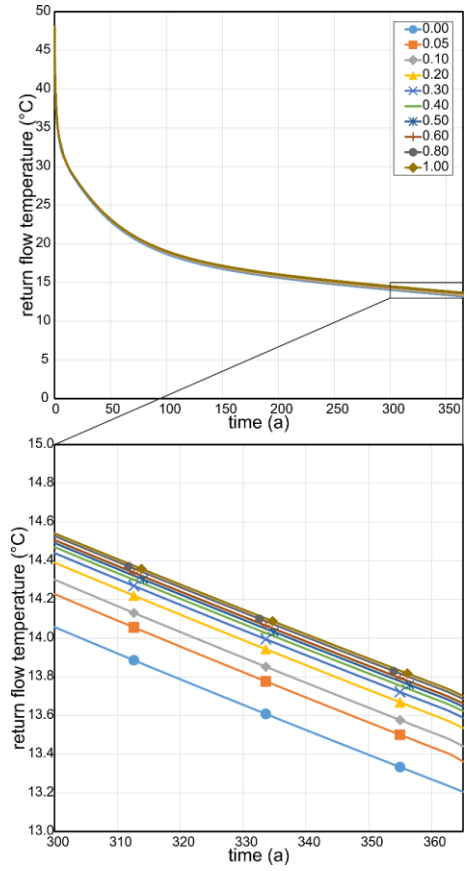

Figure 8. Return flow temperatures during heat energy extraction (phase 2) for varying thickness of a foam glass layer

5 REFERENCES

Al-Addous, M. 2006. Berechnen der Größe von Wasserspeichern zum saisonalen Speichern von Wärme bei der ausschließlichen Wärmeversorgung von Häusern mit Solarkollektoren. *Dissertation.* TU Bergakademie Freiberg.

Bach, P.-F. 2012. An energy system with seasonal storage. URL: http://www.pfbach.dk/firma_pfb/pfb_energy_system_with_seasonal_storage_2012.pdf, checked on 29.10.2018.

Baupraxis-blog 2018. Dämmstoffe. URL: http://www.baupraxis-blog.de/daemmstoffe/, checked on 29.10.2018.

Deutscher Wetterdienst 2018. Jahresgang der Globalstrahlung 2016 im Vergleich zum langjährigen Mittel 1981 - 2010 (deutschlandweites

Flächenmittel). URL: https://www.dwd.de/DE/leistungen/solarenergie/download/aktueller_jahresgang_einstrahlung.pdf?view=nasPublication&nn=16102, checked on 29.10.2018.

DHI 2015. FEFLOW 7.0 – User Guide.

Diersch, H.-J.G., Bauer, D., Heidemann, W., Rühaak, W., Schätzl, P. 2010. Finite element formulation for borehole heat exchangers in modeling geothermal heating systems by FEFLOW. *White Papers 5, 5-96*. DHI-WASY GmbH, Berlin.

Domenico, P.A.; Schwartz, F.W. 1990. *Physical and chemical hydrogeology*. Wiley, New York.

Hessisches Landesamt für Umwelt und Geologie (HLUG) 1969. Geologische Karte von Hessen; Blatt 4622 Kassel-West mit Erläuterungen.

Hultmark, G. 1982. First year operation with a seasonal storage of 80,000 m³ clay. *Workshop on solar assisted heat pumps with ground coupled storage: Proceedings. Joint Research Centre Ispra Italy* (Eds: Aranovitch, E., Hardacre, A.G., Öfverholm, E.), 433-445. Commission of the European Communities Joint Research Centre Ispra Establishment.

Hurtig, E. 1965. Untersuchungen der Wärmeleitfähigkeitsanisotropie von Sandsteinen, Grauwacken und Quarziten. *PAGEOPH 60 (1)*, 85-100.

GEOCELL 2018. Listenpreise GEOCELL, Juni 2018. URL: https://www.geocell-schaumglas.eu/fileadmin/files/GEOCELL/produkte/geocell_schaumglasschotter/download/preisliste/2018/_preisliste_allgemein_2018.pdf, checked on 29.10.2018.

Leibniz-Institut für Angewandte Geophysik (LIAG) 2016. Tiefe Geothermie - Grundlagen und Nutzungsmöglichkeiten in Deutschland. URL: https://www.geotis.de/homepage/sitecontent/info/publication_data/public_relations/public_relations_data/LIAG_Broschuere_Tiefe_Geothermie.pdf, checked on 29.10.2018.

Matthess, G., Ubell, K. 1983. Allgemeine Hydrogeologie, Grundwasserhaushalt. *Lehrbuch der Hydrogeologie Bd. 1*. (Eds. Matthess, G.). Gebrüder Bornträger, Berlin und Stuttgart.

Meteonorm 2016. Auszug der Wetterstation Standort Kassel (WMO 104380). Meteonorm v7.1.7.21517.

Midttømme, K., Roaldset, E., Aagaard, P. 1998. Thermal conductivity of selected claystones and mudstones from England. *Clay Minerals 33 (1)*, 131–145.

Nillert, P. 1976. Beitrag zur Simulation von Brunnen als innere Randbedingungen in horizontalebenen diskreten Grundwasserströmungsmodellen. *Dissertation.* Technische Universität Dresden.

Nußbicker-Lux, J. 2010. Simulation und Dimensionierung solar unterstützter Nahwärmesysteme mit Erdsonden-Wärmespeicher. *Dissertation*. Universität Stuttgart.

Ochs, F., Heidemann, W., Müller-Steinhagen, H., 2007. Langzeit-Wärmespeicher für solare unterstützte Nahwärmesysteme. *2. Internationale Speicherkonferenz Erneuerbarer Energien (IRES 2007)*, Bonn.

Ochs, F., Stumpp, H., Mangold, D., Heidemann, W., Müller-Steinhagen, H. 2004. Bestimmung der feuchte- und temperaturabhängigen Wärmeleitfähigkeit von Dämmstoffen. *OTTI, 14. Symposium Thermische Solarenergie*, Kloster Banz.

Reul, O., Räuschel, H., Schmidt, D., Orozaliev, J., Gerhold, P., Bennewitz, J. 2017. Coupling of borehole heat exchangers with solarthermal systems. *Proceedings of the 19th International Conference on Soil Mechanics and Geotechnical Engineering*, Seoul, 3463 - 3466.

SAKRET 2018. SAKRET Blähton S 10. URL: https://www.sakret.de/produkte/blahton-s-10/1617/19616, checked on 29.10.2018.

Umweltbundesamt 2017. Energieverbrauch privater Haushalte. URL: http://www.umweltbundesamt.de/daten/private-haushalte-konsum/energieverbrauch-privater-haushalte, checked on 29.10.2018.

Verein Deutscher Ingenieure (VDI) 2001a. VDI-Guideline 4640 Part 2: Thermal use of the underground, Ground source heat pumps.

Verein Deutscher Ingenieure (VDI) 2001b. VDI-Guideline 4640 Part 3: Utilization of the subsurface for thermal purposes, Underground thermal energy storage.

Verein Deutscher Ingenieure (VDI) 2010. VDI-Guideline 4640 Part 1: Thermal use of the underground, Fundamentals, approvals, environmental aspects.